USCAP

www.nature.com/labinvest

ARTICLE

Check for updates

In vitro and in vivo detection of tunneling nanotubes in normal and pathological osteoclastogenesis involving osteoclast fusion

Jing-Qi Zhang[1], Akira Takahashi[2], Jiong-Yan Gu[1], Xiaoxu Zhang[3], Yukari Kyumoto-Nakamura[1], Akiko Kukita[4], Norihisa Uehara[1], Hidenobu Hiura[1,5], Takayoshi Yamaza[1] and Toshio Kukita[1]✉

Osteoclasts are multinucleated cells formed through specific recognition and fusion of mononuclear osteoclast precursors derived from hematopoietic stem cells. Detailed cellular events concerning cell fusion in osteoclast differentiation remain ambiguous. Tunneling nanotubes (TNTs), actin-based membrane structures, play an important role in intercellular communication between cells. We have previously reported the presence of TNTs in the fusion process of osteoclastogenesis. Here we analyzed morphological details of TNTs using scanning electron microscopy. The osteoclast precursor cell line RAW-D was stimulated to form osteoclast-like cells, and morphological details in the appearance of TNTs were extensively analyzed. Osteoclast-like cells could be classified into three types; early osteoclast precursors, late osteoclast precursors, and multinucleated osteoclast-like cells based on the morphological characteristics. TNTs were frequently observed among these three types of cells. TNTs could be classified into thin, medium, and thick TNTs based on the diameter and length. The shapes of TNTs were dynamically changed from thin to thick. Among them, medium TNTs were often observed between two remote cells, in which side branches attached to the culture substrates and beaded bulge-like structures were often observed. Cell-cell interaction through TNTs contributed to cell migration and rapid transport of information between cells. TNTs were shown to be involved in cell-cell fusion between osteoclast precursors and multinucleated osteoclast-like cells, in which movement of membrane vesicles and nuclei was observed. Formation of TNTs was also confirmed in primary cultures of osteoclasts. Furthermore, we have successfully detected TNTs formed between osteoclasts observed in the bone destruction sites of arthritic rats. Thus, formation of TNTs may be important for the differentiation of osteoclasts both in vitro and in vivo. TNTs could be one target cellular structure for the regulation of osteoclast differentiation and function in bone diseases.

Laboratory Investigation (2021) 101:1571–1584; https://doi.org/10.1038/s41374-021-00656-9

INTRODUCTION

Bone metabolism is maintained by a dynamic balance between bone resorption mediated by osteoclasts and bone formation mediated by osteoblasts[1,2]. Osteoclasts are large multinucleated giant cells derived from hematopoietic stem cells. These unique cells specialized for bone resorption are differentiated under the specified bone microenvironments mainly consisted of receptor activator NF-κB ligand (RANKL) and macrophage colony-stimulating factor (M-CSF)[3,4]. Under the bone microenvironments, osteoclast progenitors derived from hematopoietic stem cells are differentiated into mononuclear osteoclast precursors, which recognize each other to form multinucleated osteoclasts through cell-cell fusion[5–7]. However, details of the cell-cell fusion events in osteoclasts are not fully described.

Rustom et al[8]. first reported nano-scale tubular structures formed between rat pheochromocytoma PC12 cells and normal rat kidney NRK cells, in which authors designated the new type of cell-cell connection as the membrane or tunneling nanotubes (TNTs). TNTs are involved in intercellular communication, based on the formation of thin tunnels, between homologous or heterologous mammalian cells. In general, TNTs have diameters of 25–200 nm and lengths of over several cell diameters between remote cells, in which fine tunnel-like membrane structures involving F-actin filaments are connecting remote cells[8–11]. Recently, TNTs and related structures have attracted attention as the important fine cellular structure for mediating rapid cell-cell communication in various kinds of cells, including human dendritic cells, monocytes, natural killer cells, macrophages, human endothelial progenitor cells, neonatal rat cardiomyocytes, and rat astrocytes[12–16]. Intercellular transport of signaling molecules, membrane vesicles, intracellular organelles, and cell-surface molecules between remote cells is carried out through TNTs. TNTs are associated with various cellular events involving cell migration, transcytosis, cell fusion, and cell differentiation[8,9,15,17,18]. TNTs are also involved in the pathogenesis of various diseases, including cancers and infectious

[1]Department of Molecular Cell Biology and Oral Anatomy, Division of Oral Biological Sciences, Faculty of Dental Science, Kyushu University, Fukuoka, Japan. [2]Department of Fixed Prosthodontics, Division of Oral Rehabilitation, Faculty of Dental Science, Kyushu University, Fukuoka, Japan. [3]Department of Implant and Rehabilitative Dentistry, Division of Oral Rehabilitation, Faculty of Dental Science, Kyushu University, Fukuoka, Japan. [4]Department of Research Center of Arthroplasty, Faculty of Medicine, Saga University, Saga, Japan. [5]Department of Orthodontics and Dentofacial Orthopedics, Division of Oral Health, Growth, and Development, Faculty of Dental Science, Kyushu University, Fukuoka, Japan. ✉email: kukita.toshio.433@m.kyushu-u.ac.jp

Received: 4 March 2021 Revised: 4 August 2021 Accepted: 4 August 2021
Published online: 18 September 2021

diseases[9,19,20]. TNTs are utilized in communication between host cells with pathogenic organisms. Pathogenic *E. coli* extracts nutrients from infected host entero-epithelial cells by use of newly formed TNTs, which are generated by the injectisome of the *E. coli*[21].

In the previous study, we reported the appearance of numerous TNTs in osteoclast differentiation, especially in the fusion process of osteoclast precursors in osteoclast differentiation in vitro, and we also clarified a rapid transfer of dendritic cell-specific transmembrane protein (DC-STAMP), a transmembrane molecule essential for cell fusion in osteoclastogenesis, through TNTs[22,23]. Recently, Li et al. reported the presence of TNTs in the coculture system of osteoclast precursors and endothelial progenitors[24]. They showed suppression of osteoclast formation by macrophage migration inhibitory factor released from endothelial progenitor cells through TNTs. Pennenen et al. reported the presence of nuclei in TNT-like structure observed in human osteoclast cultures, suggesting that intracellular structures including intracellular organelles and nuclei could migrate into TNTs[25]. Thus, TNTs are considered to be utilized for transmitting information between remote cells during osteoclastogenesis.

Although formation of TNTs is associated with the process of osteoclast differentiation, the precise morphological features of TNTs has not yet been reported and it is not known whether TNTs associate with osteoclasts in vivo. In order to address more precise involvement of TNTs in osteoclastogenesis and their contribution in maintaining bone homeostasis, we analyzed detailed morphology of TNTs observed in osteoclastogenesis involving cell-cell fusion process by use of scanning electron microscopy (SEM) and fluorescence microscopy. We also searched for TNT-like structures in pathological osteoclastogenesis in bone destruction sites of adjuvant-induced arthritis (AA) in rats. Here we clarified the dramatic changes in the cell surface morphology of osteoclast precursors after being stimulated to form multinucleated osteoclasts. We have defined three types of TNTs in osteoclastogenesis and observed numerous nuclei in TNTs during the fusion process of osteoclast-like cells. We also detected TNT-like structures in osteoclasts formed in bone destruction sites of AA in rats.

MATERIALS AND METHODS

Animals and reagents

Male C57BL/6 mice (5–7 weeks old) and male Lewis (LEW/SsN) rats (5 weeks old) were purchased from Kyudo (Tosu, Japan) and were used for murine bone marrow culture for osteoclastogenesis and for induction of adjuvant-induced arthritis (AA), respectively. All animal experiments were performed according to the protocol approved by the Laboratory Animal Care and Use Committee of Kyushu University (Permission Number: Kyushu Univ. Res. No. A19-270-0).

Recombinant human M-CSF and recombinant human soluble RANKL were obtained from PeproTech (Rocky Hill, NJ). Heat-killed *Mycobacterium butyricum* and mineral oil were obtained from Difco Laboratories (Detroit, MI). Alpha-minimum essential medium (α-MEM), fetal bovine serum (FBS), penicillin, streptomycin glutamine (100×) and TrypLE Select (10×) were obtained from Life Technologies (Grand Island, NY). Acti-stain™ 488 Fluorescent Phalloidin was obtained from Cytoskeleton, Inc (Denver, CO). Mouse anti-Cathepsin K antibody (sc-48353) was obtained from Santa Cruz Biotechnology (Santa Cruz, CA). Goat anti-mouse IgG (H + L) conjugated with Alexa Fluor 568 was obtained from Invitrogen (Waltham, MA), and 4′,6-diamidino-2-phenylindole (DAPI) was purchased from Sigma-Aldrich (St Louis, MO). Tartrate-resistant acid phosphatase (TRAP) assay kit was obtained from Sigma-Aldrich (St Louis, MO). Small columnar dentin pieces were purchased from Asashima-Ryubundo (Fukuoka, Japan).

Cell culture and osteoclastogenesis

Osteoclast differentiation from osteoclast precursor cell line RAW-D cells. Osteoclast-like cells were differentiated from murine osteoclast precursor cell line RAW-D (a subclone of RAW264 cells) as described previously[23,26–28]. Briefly, RAW-D cells were cultured in 96-well plates (6.75×10^3 cells per well) for 4 days in α-MEM containing 10% FBS in the presence of 50 ng/ml RANKL. Cultured cells were stained for osteoclast marker enzyme TRAP according to the manufacturer's protocol as described previously[23,26]. TRAP positive cells bearing more than three nuclei were counted as multinucleated osteoclast-like cells.

Osteoclast differentiation from murine bone marrow cells. Murine osteoclast-like cells were differentiated from bone marrow macrophages (BMMs) prepared from bone marrow cells obtained from tibia and femur of C57BL/6 mice as described by Takahashi et al.[28]. Murine bone marrow cell culture was performed as described previously[29,30]. In brief, bone marrow cells were cultured in the presence of M-CSF (10 ng/ml) for 3 days to obtain BMMs followed by being stimulated by RANKL (50 ng/ml) and M-CSF (10 ng/ml) for 2 days. BMMs were detached from the culture dish with TrypLE Select and cells (1.5×10^5 cells/ml, 2 ml) were replated on dentin slices and further cultured with RANKL (50 ng/ml) and M-CSF (10 ng/ml) for more 2 or 3 days.

Induction of adjuvant-induced arthritis in rats

Rats with AA were prepared as described previously[31]. Briefly, 5 weeks old male Lewis rats were anesthetized with isoflurane inhalation and were intradermally injected with complete Freund adjuvant containing 25 mg/kg heat-killed *Mycobacterium butyricum* (Difco Laboratories, Detroit, MI) suspended in mineral oil at the base of the tail. For the control experiments, rats were injected with mineral oil alone. The rats were killed on day 21 after the adjuvant injection and processed for immunohistochemical analysis.

Immunofluorescence staining of bone and cultured osteoclasts

After anesthetizing with isoflurane inhalation followed by intraperitoneal injection of pentobarbital (1 mg/kg body weight), the rats were aseptically dissected and fixed by perfusion with 4% paraformaldehyde (PFA) in PBS (pH 7.4) from the left ventricle. Ankle joints were excised from the hind paws and immersed in the same fixative for overnight at 4 °C, followed by washing in PBS. After decalcification in 10% (w/v) ethylene diamine tetraacetic acid disodium salts (EDTA-2Na) for 3 weeks at 4 °C, tissue blocks were immerged in sucrose series (10–40%) in PBS overnight and then embedded in optimal cutting temperature (OCT) compound. Cryosections (10 μm) of ankle joints with tibia-tarsal-calcaneus bones were prepared by use of the cryostat HM560MV (Zeiss, Oberkochen, Germany). Sections were completely dried up at room temperature and immersed in PBS to remove the OCT compounds. For the immunofluorescent staining of cultured cells, cultured RAW-D cells on coverslips were fixed in 4% PFA in PBS and processed for immunofluorescence staining.

Specimens were rinsed in 10 mM glycine in PBS to quench unreacted aldehyde groups and were blocked in 5% chicken albumin in PBS for 60 min at room temperature followed by further blocking in 10% goat serum in PBS for 60 min in a moisture chamber at room temperature. Specimens were incubated with a mixture of Acti-stain™ 488 Fluorescent Phalloidin (1:40 dilution) to detect F-actin filaments and anti-Cathepsin K antibody (1:50 dilution) or control IgG at room temperature for 4 h in a moisture chamber. After washing with PBS, specimens were incubated with goat anti-mouse IgG (H + L) antibody conjugated with Alexa Fluor 568 (diluted 300 times in 1% BSA in PBS) for 30 min in a dark moisture chamber. After washing with PBS, nuclei were stained with DAPI (1:50 dilution) for 1.5 min in a dark moisture chamber. After rinsing in PBS, specimens were mounted in Aqua-Poly/Mount (Polysciences Inc., Washington, PA) for observation by use of BZ-X800 fluorescence microscope (Keyence, Osaka, Japan) and Apotome 2 microscopy (Zeiss, Oberkochen, Germany). Two- and three-dimensional images of the cells were obtained and analyzed using BZ-X800 analyzer version 1.1.10 software (Keyence, Osaka, Japan) and ZEN version 2.6 software (Zeiss, Oberkochen, Germany).

Scanning electron microscopy

The RAW-D cells stimulated with RANKL (50 ng/ml) were cultured on coverslips for 3 and 4 days. Murine BMMs-derived osteoclasts were replated on dentin slices as described above. For analyzing by SEM, cells were fixed with 2.5% glutaraldehyde in 0.1 M sodium cacodylate buffer (pH 7.4) for 30 min at 4 °C followed by the post-fixation with 1% osmium tetroxide in 0.1 M sodium cacodylate buffer for 1 h at 4 °C. After rinsing in PBS, cells were dehydrated in a graded ethanol series and immersed in *t*-butyl alcohol, followed by freeze dried using freeze-drying equipment (JFD-300, JEOL, Tokyo, Japan). After sputter-coating with Au-Pd

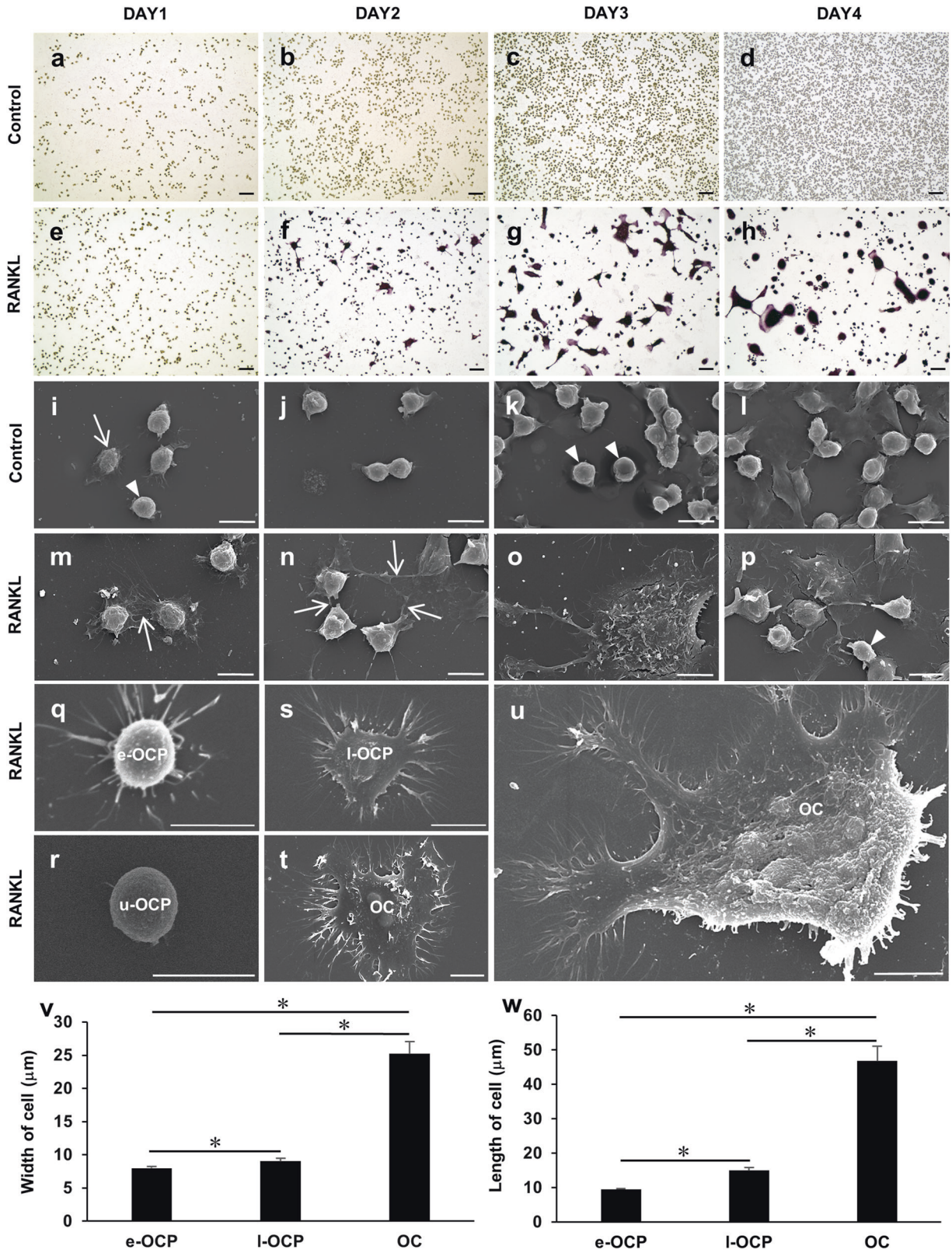

by Magnetron Sputter (MSP-1S, Vacuum Device, Ibaraki, Japan), cells were examined by SEM (S-3400N, Hitachi, Tokyo, Japan) at 15kV and digital images were collected. The size of osteoclasts and the diameter and length of TNTs were measured from the photographed images using ImageJ version 1.8 software (National Institutes of Health, Bethesda, MD).

Statistical analysis

All data were expressed as mean ± standard error of the mean (SEM) from at least three independent experiments. The size of osteoclasts and the diameter and length of TNTs were measured as described above. Statistical significance between two and multiple groups was determined by using

Fig. 1 Time-course of osteoclast differentiation and morphological classification of cells observed in osteoclast precursor cell line RAW-D. RAW-D cells were cultured by day 4 in the presence or absence of RANKL followed by TRAP staining (**a–h**) or SEM analysis (**i–p**) as described in Materials and Methods. **a–h** TRAP-positive osteoclast-like cells were formed when cells were stimulated with RANKL (50 ng/ml) (**e–h**) but no osteoclast-like cells were formed in the absence of RANKL (control) (**a–d**). **i–p** SEM observations of the same culture. In control groups (**i–l**), few (arrow) or no protrusions (arrowheads) were observed. TNT-like structures were frequently detected when cells were stimulated to form osteoclasts, in which numerous thin protrusions were observed (arrows) (**m–p**), few cells without cellular protrusions were also observed (**p** arrowhead). These cells can be classified into following groups according to the cell size, morphology, number of nucleus and cell volume. **q** Spheroid small cells with protrusions (early osteoclast precursors; e-OCP). **r** Spheroid small cells without protrusions (undifferentiated osteoclast precursors; u-OCP). **s** Flat mononuclear cells with many protrusions (late osteoclast precursors; l-OCP). **t** Small multinucleated osteoclast-like cells (OC). **u** Large multinucleated osteoclast-like cells (OC). **v**, **w** Quantitative demonstration of the width (**v**) and length (**w**) of each osteoclast precursors and osteoclast-like cells. Values represent mean ± SEM from at least three independent experiments. *$P < 0.05$ ($n = 50$). Scale bars: 100 μm (**a–h**), 10 μm (**i–u**).

paired Student's *t* test and one-way analysis of variance (ANOVA). Values of $P < 0.05$ were considered as statistically significant.

RESULTS

Morphological changes and characteristics of mononuclear osteoclast precursors and multinucleated osteoclast-like cells in RAW-D cells during osteoclastogenesis

The osteoclast precursor cell line RAW-D cells were stimulated by RANKL to form osteoclast-like cells, followed by staining for TRAP and observed by optical microscopy and SEM. Figure 1a–h shows the morphological changes in cells in osteoclastogenesis stained with TRAP over time. Detailed surface morphological changes in these cells were analyzed by SEM (Fig. 1i–p). A large number of TRAP-positive mononuclear osteoclast precursors were observed from 2 days after stimulation by RANKL, many of which stretch thin protrusions and connect with adjacent cells through thin protrusions (Fig. 1m, n, arrows). Cells bearing a few (Fig. 1i, arrow) or no protrusions (Fig. 1i, k, p, arrowheads) were also observed. These spheroid mononuclear cells with or without cellular protrusions are supposed to be the early osteoclast precursors (e-OCP). Numbers of multinucleated osteoclast-like cells having more than three nuclei were markedly increased and reached to the maximum level at 3 days of culture (Fig. 1g, o). Based on the morphological characteristics, we classified these cells into three types of cells with different morphology. The first cell type is the e-OCP, mononuclear cells bearing spheroid morphology with numerous thin cellular protrusions (Fig. 1q), although sometimes, spheroid mononuclear cells having no protrusion are observed (Fig. 1r). As mononuclear cells with no protrusion showed similar morphology as that of unstimulated RAW-D cells (Fig. 1i-l), these cells are thought to be 'undifferentiated osteoclast precursors' (u-OCP). In contrast, small round e-OCP cells with thin protrusions are supposed to be more differentiated cells. These OCPs have an average width of 8.0 μm (5.9–13.8 μm) and the average length of 9.5 μm (6.4–14.5 μm) (Fig. 1q, r, v, w). The second cell type is a slightly bigger flat mononuclear cell with numerous medium-size protrusions, which are believed to be more differentiated cells called 'late osteoclast precursors' (l-OCP) (Fig. 1s). These mononuclear cells have an average width of 9.1 μm (5.6–20.0 μm) and the average length of 15.0 μm (6.9–43.9 μm) (Fig. 1s, v, w). The third cell type is the 'multinucleated osteoclast-like cells' (OC), which was observed somewhat much bigger and irregular cells with medium or thick size protrusions and bearing three or more nuclei (Fig. 1t). These multinucleated cells are supposed to be mature osteoclast-like cells. Interestingly, numerous protrusions with fine side branches were observed in these cells. Figure 1u shows a typical multinucleated osteoclast-like cells with large size, having numerous protrusions with fine side branches. These multinucleated osteoclast-like cells have an average width of 25.2 μm (4.9–140.0 μm) and the average length of 46.8 μm (16.1–186.7 μm) (Fig. 1t–w). The different cell types observed in culture of osteoclastogenesis are as follows: (i) e-OCP bearing spheroid morphology with numerous thin cellular protrusions or u-OCP with no protrusions; (ii) l-OCP, mononuclear cells with flat and irregular shape bearing numerous thin or medium-size protrusions; (iii) multinucleated osteoclast-like cells (OC), bearing three or more nuclei with numerous medium or thick size protrusions. As shown in Fig. 1v, w, both width (Fig. 1v) and length (Fig. 1w) of cells were significantly increased in multinucleated osteoclast-like cells if compared with e-OCP and l-OCP.

Type of the protrusion in osteoclast lineage

Under culture conditions for osteoclastogenesis, numerous cells were connected to adjacent or distant cells via short or long protrusions (Fig. 2a–k). Numerous thin spinous processes around the cells were observed in e-OCP (Fig. 2a, b). Spheroid cells tended to extend long protrusions, which also could be called as filopodia (Fig. 2c), or lamellipodia (Fig. 2d). Interestingly, these cellular protrusions possessed several fine side branches, which attached to the culture substrates (Fig. 2c, d, arrowheads). These long protrusions had similar morphology with nerve axons and extended up to 120 μm (Fig. 2e, arrows). Such cellular protrusions occasionally reached to more than 200 μm in their length (data not shown). The number of such cell protrusions per one cell varied from one to several (Fig. 2f–k). We speculate that these long protrusions and side branches are not only involved in connection with distant cells and signal-transport between the cells in the osteoclast lineage but also in the modulation of osteoclast differentiation and migration.

Detection of TNTs between osteoclast precursors in culture and classification of TNTs

Osteoclast precursor cell line RAW-D cells were stimulated with RANKL to form osteoclast-like cells from day 1 to day 4 of culture (Fig. 1e–h, m–p). The detailed surface morphology of cells was observed by use of SEM (Fig. 3a–g). A large number of osteoclast precursors were observed from day 2 (Fig. 3a) after RANKL-stimulation and numbers of multinucleated osteoclast-like cells were markedly increased on day 3 (Fig. 3c). Osteoclast precursors and osteoclast-like cells stretched thin protrusions or TNTs to connect with adjacent cells (Fig. 3a–e). Typical TNTs were observed between spheroid e-OCP in Fig. 3b, d.

Based on the size of TNTs and morphological characteristics of connected cells, we also classified three types of TNTs observed in osteoclastogenesis. Figure 3e–g shows the typical SEM image of each type of TNTs. The first type is the 'thin nanotubes' bearing average diameter of 298 nm (140–770 nm) with the average length of 11.2 μm (1.4–31.6 μm) (Figs. 3a–e, 3h, i). This type of TNTs was frequently observed between e-OCP. One or multiple thin nanotubes were observed among the osteoclast precursors. This type of TNTs tended to be short and straight (Fig. 3a–e). The second type is 'medium nanotubes' of average diameter 778 nm (210 nm–1.5 μm) with an average length of 45 μm (9.3–98 μm) (Fig. 3f, h, i). This type of TNTs was frequently associated with l-OCP and small-sized multinucleated osteoclast-like cells. The medium nanotubes mainly bridged two cells located in a long distance from each other. Several fine side branches were observed in this type (Fig. 3f, arrowheads). The third type is the

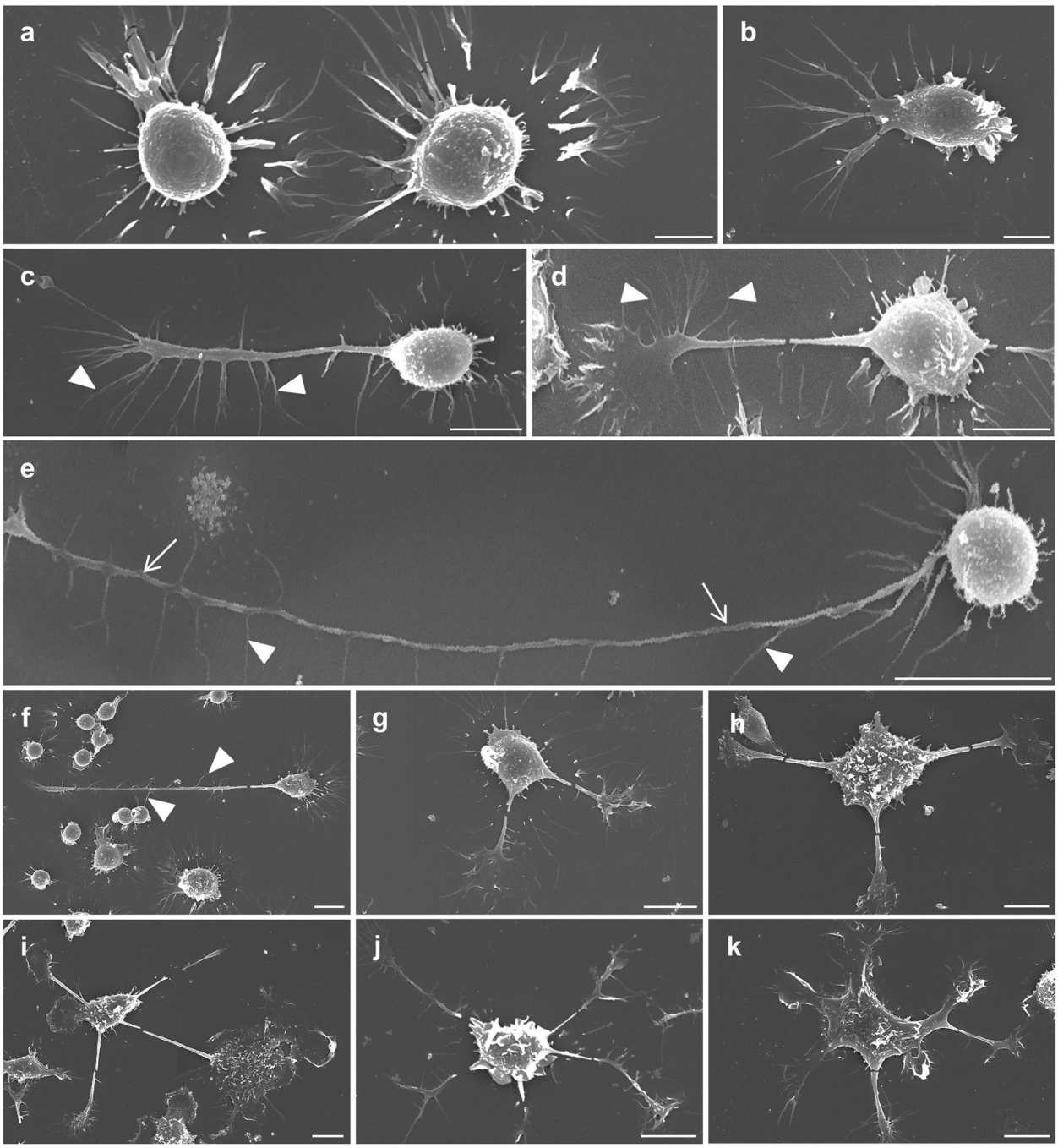

Fig. 2 Various types of cellular protrusions observed in culture of osteoclastogenesis by SEM analysis. Osteoclast precursors have various types of cellular protrusions. In osteoclast precursors, (**a**) radial or (**b**) octopus-like, (**c**) filopodia, and (**d**) lamellipodia-like protrusions were observed. A long protrusion similar to nerve axon was observed (arrows) (**e**). **c–f** Some medium-long unipolar protrusions with numerous fine side branches (arrowheads), (**g**) bipolar or (**h–k**) multipolar protrusions were also observed. Scale bars: 5 μm (**a**, **b**), 10 μm (**c**, **d**, **f–k**), 20 μm (**e**).

'thick nanotubes' with thick in diameter and shorter in length bearing the average diameter of 2.5 μm (420 nm–18.8 μm) with an average length of 35.5 μm (9.1–106.4 μm) (Fig. 3g, h, i). This type of TNTs was observed between l-OCP and multinucleated osteoclast-like cells. Only a few side branches were observed in this type of TNT (Fig. 3g). The thicker TNT connecting two osteoclast-like cells also could be called as the TNT-like intercellular bridge. As shown in Fig. 3, both diameter (Fig. 3h) and length (Fig. 3i) of TNTs were significantly longer in medium and thick nanotubes than those of thin nanotubes. There was no significant difference in the length of medium nanotubes and thick nanotubes.

The detailed morphology of TNTs and various fine side branches in TNTs

Concerning the detailed surface morphology of TNTs in osteoclastogenesis, as we could not observe any special synapse-like structures at the connected portion between the cell body and TNTs (Fig. 4a, area 1 and 3), these TNTs are open-ended TNTs. In the middle portion of TNTs, it was sometimes observed a few beaded bulges (Fig. 4a, area 2), which could be related to the structure for the transport of some intracellular organelles or membrane vesicles between connected cells through TNTs.

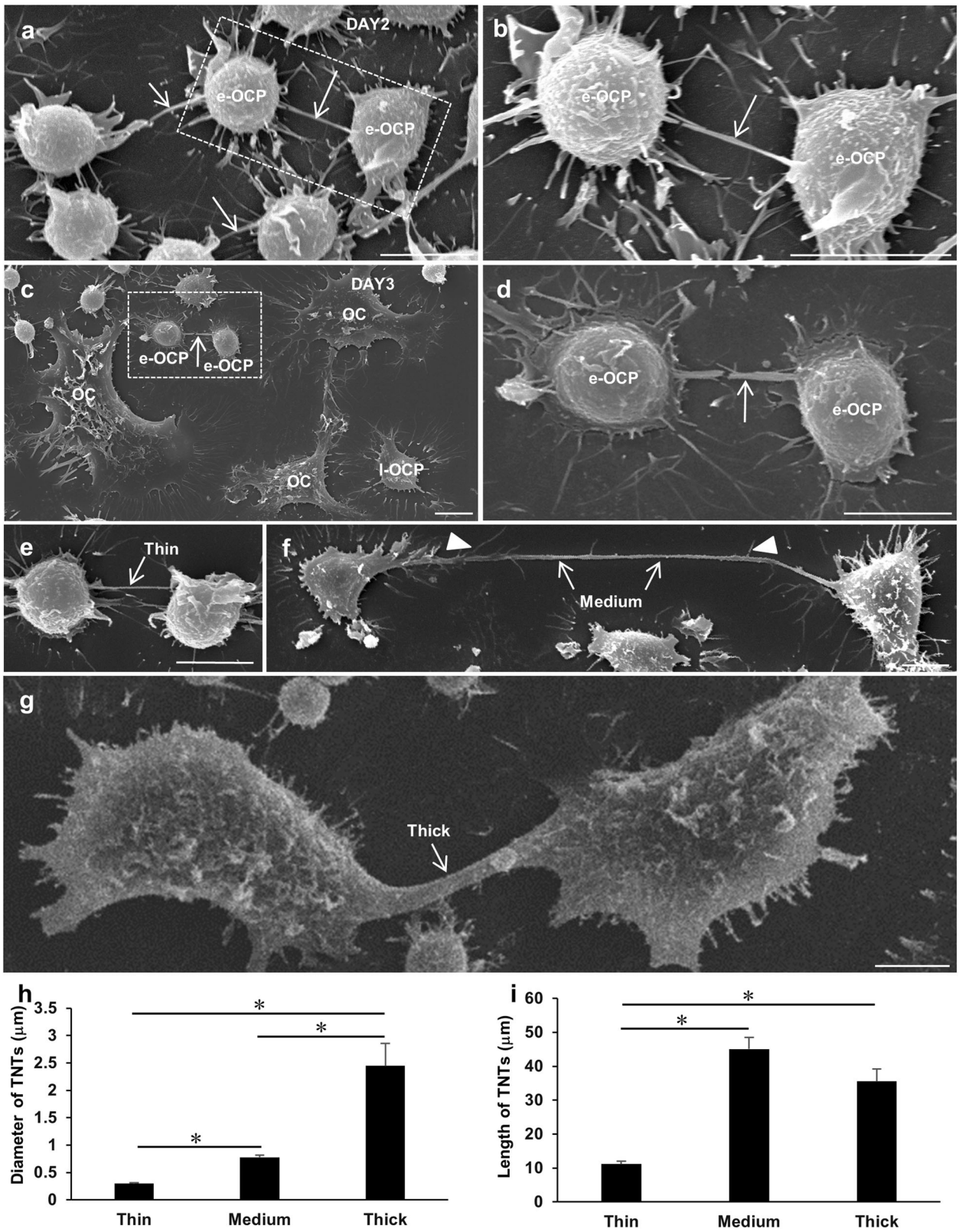

Among the TNTs, especially in medium nanotubes, it was observed the long TNTs formed between cells present far away from each other. The shapes of TNTs were observed to be straight (Fig. 4b) and parts of them were curved (Fig. 4c). Several fine side branches were seen in this type of TNTs (Fig. 4b, c, arrows), which branched from the main trunk of TNTs. A part of such side branches was directly connected with adjacent cells (Fig. 4d, arrows). TNTs were frequently formed between specific two cells locating far away from each other, but without forming any connections to the adjacent cells which present between these

Fig. 3 Appearance of TNTs in culture cells and classification of TNTs by SEM analysis. SEM observation of TNT-like structures in 2 days (**a**) and multinucleated osteoclast-like cells (**c**) in 3 days of cultured RAW-D cells in osteoclastogenesis. **b** and **d** are high magnification views of the boxed areas in (**a** and **c**), respectively. Arrows show TNT-like structures formed in cultured osteoclast precursors. TNTs were classified into three types based on the diameter, length, morphology, and connected cell characteristics; **e** Small diameter nanotubes (Thin nanotubes): Thin nanotubes were observed mainly in small early osteoclast precursors. Straight and less branched TNTs were observed (arrow). **f** Middle diameter nanotubes (Medium nanotubes): Medium nanotubes were present in small or medium sized late osteoclast precursors or small-sized multinucleated osteoclast-like cells, which were observed as one relatively longer and thicker tube (arrows). Fine branches were observed in these TNTs (arrowheads in **f**). **g** Large diameter nanotubes (Thick nanotubes): Thick nanotubes were observed between two multinucleated osteoclast-like cells. These TNTs are thick and slightly shorter (arrow). **h**, **i** Quantitative demonstration of the three types TNTs observed in osteoclastogenesis: Difference in the diameter (**h**) and the length (**i**) of TNTs. Values represent mean ± SEM from at least three independent experiments. $*P < 0.05$ ($n = 50$). e-OCP: early osteoclast precursor. l-OCP: late osteoclast precursor. OC: multinucleated osteoclast-like cell. Scale bars: 10 μm (**a–g**).

specified cells (Fig. 4e, f, arrowheads). In respect to cell-cell connection, the several modes of connections were observed. The first type of connection was by using the tips of long filopodia, in which one or two cells stretch protrudes with one long TNT (Fig. 4g). The second type of connection was through lamellipodia, in which two cells extend each long-elongated protrusion bearing lamellipodia structure on tip of the process and bind to each other (Fig. 4h). The third type of connections between cell processes was to form multiple connections with multiple cells as shown in Fig. 4i, in which a long TNT-like structure formed between cells of far distance made connection with three small spheroid cells. Such structures may be related to the efficient communication among multiple cells through TNT-like structure.

TNTs may be involved in cell-cell fusion and formation of multinucleated osteoclast-like cells

The following morphological events may be involved in the process of cell-cell fusion observed in the multinucleation step in osteoclastogenesis: A possible first step is the formation of TNTs between two mononuclear osteoclast precursors (Fig. 5a), in which TNTs become thicker and shorter, and some small cells were more likely to fuse toward the main large cell (Fig. 5b) possibly followed by cell-cell fusion as a possible second step. Figure 5c shows the third step, a possible critical moment of cell-cell fusion by thick intracellular bridges formed between osteoclast-like cells. Figure 5d shows the typical multinucleated osteoclast-like cells, in which large osteoclast-like cells bearing multiple nuclei protrude short protrusion toward the periphery of the cell. TNT-like structure was also observed between an early osteoclast precursor and a small osteoclast-like cell (Fig. 5e) or between the multinucleated osteoclast-like cell and the late osteoclast precursor in culture (Fig. 5f), demonstrating that TNT-mediated intercellular communication is likely to be important in the cell fusion process of osteoclast formation. In the vicinity of multinucleated osteoclast-like cells, we observed a cluster of e-OCP connected with each other by short TNT-like structures which were likely to be the intercellular connections among the e-OCP (Fig. 5g). TNTs formed between the multinucleated osteoclast-like cell and the early osteoclast precursor were also observed (Fig. 5g). These e-OCP also could be accumulated and clustered to fuse each other. It is well known that the smaller size of osteoclasts fuses each other to form larger osteoclasts. Figure 5h demonstrate fusion between two multinucleated osteoclast-like cells, in which a direct plasma membrane contact area (approximately 10 μm width) was observed. Interestingly, several TNT-like intercellular bridges were observed just close to the membrane fusion area, which could guarantee the efficient membrane fusion between osteoclast-like cells (Fig. 5h).

A possible transfer of vesicular components and nuclei through TNTs in osteoclastogenesis

TNTs, F-actin based intercellular bridge-like structures connecting adjacent cells, were detected by fluorescent phalloidin. The cellular processes of osteoclasts were also detected by showing the presence of cathepsin K, a marker of osteoclasts. Figure 6 shows the double detection of F-actin and cathepsin K in TNTs observed in osteoclastogenesis in RAW-D cell cultures. Relatively medium and thick TNT were observed between two multinucleated osteoclast-like cells (Fig. 6a–h). In the observed TNT formed between two osteoclast-like cells, F-action (Fig. 6a, e, green) and cathepsin K (Fig. 6b, f, red) were detected. DAPI stained numerous nuclei were present in the multinucleated osteoclast-like cells (Fig. 6c, g, blue). In previous studies, we reported that TNT could transport not only membrane phospholipids but also cell surface proteins[22]. In the present study, cathepsin K-positive vesicular components were present in the medium size TNT formed between osteoclast-like cells (Fig. 6b, arrows), suggesting that vesicular components were transferred between two osteoclast-like cells through TNT. Interestingly, thick or large TNTs adjacent to multinucleated osteoclast-like cells were found (Fig. 6e–h), and several nuclei were observed also in TNT (Fig. 6f–h, inset of three-dimensional view in Fig. 6h). These results clearly demonstrate the actual transfer of nuclei through TNTs formed between connected cells in the osteoclast-lineage.

Detection of TNTs in cultures of primary osteoclasts on dentin slices

To confirm the morphology and function of TNT-like structures in primary osteoclasts, we examined the surface morphology of the primary osteoclasts cultured on dentin slices. BMM-derived primary osteoclasts formed under stimulation with RANKL and M-CSF were replated on dentin slices. Small-sized osteoclasts bearing numerous fine protrusions (Fig. 7a) and larger-sized osteoclasts with irregular shape (Fig. 7b) were observed on dentin slices. Figures 7c and 7d show TNTs observed between two osteoclasts possibly migrating on the surface of dentin. Several resorption lacunae were observed on the surface of the dentin slices (Fig. 7d–h, arrowheads). The osteoclasts were adhered to the surface of the dentin and underlying resorption lacuna was observed under beneath of the osteoclast (Fig. 7e, f). Many small and large typical resorption lacunae were formed on the surface of the dentin, in which the collagen fibrils were exposed at the bottom of the resorption lacunae (Fig. 7d–h).

In vivo detection of TNTs in inflammatory bone destruction sites in adjuvant-induced arthritic rats

To confirm the presence of TNT-like structures in the pathological bone destruction sites in arthritic rats, we have carefully searched the TNTs associated with osteoclasts in the ankle joint sections of rats with AA. Severe bone destruction and marked elevation of osteoclastogenesis were observed in the talus of arthritic rats (Fig. 8a). The immunofluorescence staining of the ankle joint tissues using the Fluorescent Phalloidin (green) and anti-cathepsin K antibody (red) revealed that F-actin containing TNT-like structures, which also contain cathepsin K, were frequently observed between multinucleated osteoclasts in the pathological bone destruction sites (Fig. 8b–f). Inset in Fig. 8f is the three-dimensional view of the TNT formed between two multinucleated

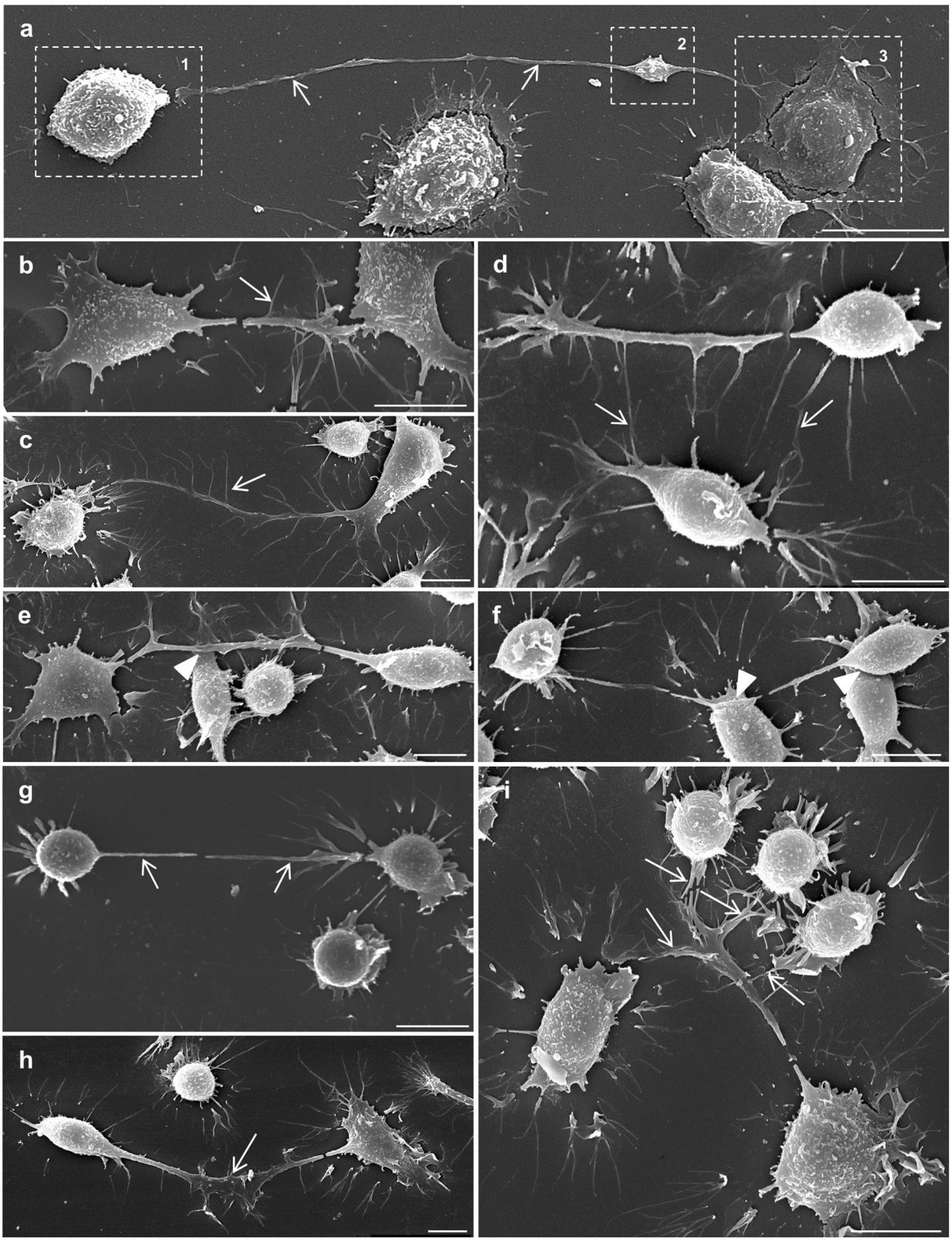

Fig. 4 Detailed morphology of TNTs and various fine side branches associted with TNTs connecting cells. a Typical morphology of TNT formed between two osteoclast precursors (arrows). Boxed areas of (**a1**, **3**) were shown no special synapse-like structures between the cell body and TNT. Formation of the beaded bulge-like structure was observed in TNT boxed area of (**a2**). **b**, **c** The course of TNTs between osteoclast precursors or osteoclasts is straight or curved. In addition to the connection between the cells as the intercellular bridge, several fine side branches were observed in each TNT (**b–d** arrows). **d** A part of which was connected to the adjacent cells (**d** arrows). **e**, **f** Some TNTs were likely to pass-through on some cells without forming direct connections (arrowhead). Some TNTs connected two cells directly by using tips of each filopodia (**g** arrows) or using lamellipodia-like tips (**h** arrow). Some TNTs connected with multiple osteoclast precursors through fine side branches (**i** arrows). Scale bars: 10 μm (**a–i**).

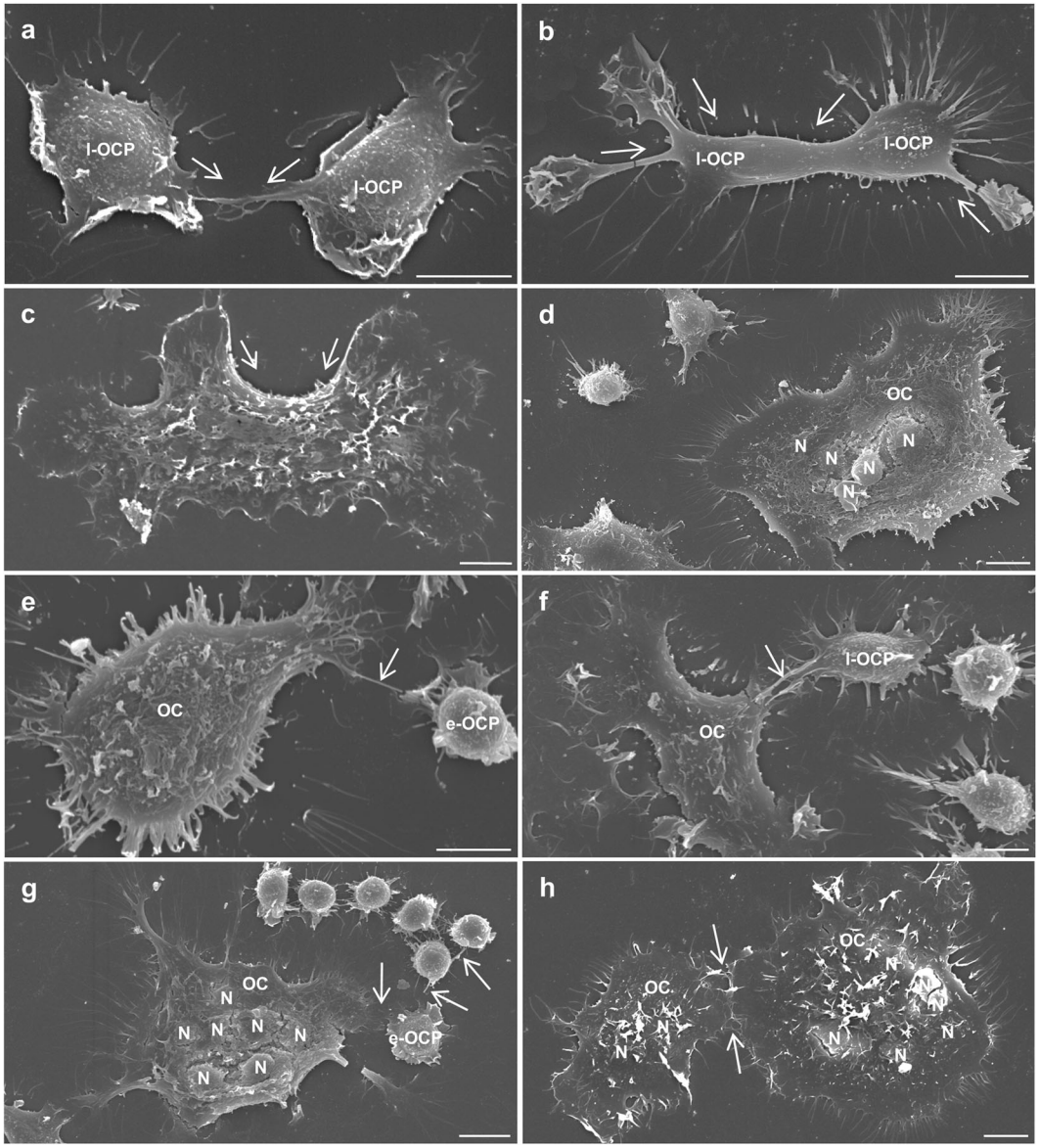

Fig. 5 Association of TNTs in the process of cell fusion in osteoclastogenesis. a–d SEM analysis showed the cell fusion was generated through the fusion among late osteoclast precursors (**a**). As a possibility of the fusion process, TNTs formed between osteoclast precursors could become thicker and shorter just before cell fusion followed by fusion with each other to form multinucleated osteoclast-like cells (**b–d**). Arrows show the possible direction of cell-cell fusion by TNT-like structures (**a–c**). **e–g** To form larger osteoclasts, osteoclast-like cells were connected to the surrounding mononuclear osteoclast precursors via TNTs (**e**–**g** arrows). The TNT observed between the osteoclast precursors and the multinucleated osteoclast-like cell (**e**, **f** arrow). Short TNT-like structures formed between the multinucleated osteoclast-like cell and a cluster of osteoclast precursors in which cells are connected with each other (**g** arrows). **h** Demonstration of fusion between two multinucleated osteoclast-like cells, in which it was observed the direct plasma membrane contact associated with fine TNTs (arrows) in the vicinity of the fusion site. e-OCP: early osteoclast precursor. l-OCP: late osteoclast precursor. OC: multinucleated osteoclast-like cell. N: nucleus, Scale bars: 10 μm (**a–h**).

osteoclasts in the pathological bone destruction sites. These data strongly suggest the actual presence of TNTs in vivo.

DISCUSSION

In the present study, we show that TNTs are involved in the fusion process in osteoclast differentiation. Based on the morphological characteristics of cells in osteoclast lineage, we classified cells observed in osteoclastogenesis into three types: (i) e-OCP which include u-OCP, (ii) l-OCP and (iii) multinucleated osteoclast-like cells (OC). Furthermore, we observed that TNT-like structure was formed between the osteoclast-like cells, and the morphology of each TNT was found to be different depending on the type of connected cells. Importantly, TNT was involved in the transport of intracellular molecules and osteoclast fusion, in which membrane components, cytoplasmic molecules, organelles, and even nuclei, were being transported through TNTs. We also confirmed the formation of TNTs between primary osteoclasts resorbing dentin in vitro. Furthermore, we have successfully detected TNT-like structure in vivo, in which we have found TNT-like intercellular bridges connecting osteoclasts abundantly present in bone destruction sites of rats with AA. We have previously reported that these osteoclasts bear high TRAP activity, high level of Cathepsin K and high level of osteoclast specific Kat1 antigen as well as high bone resorbing activity[32,33]. These in vivo data strongly suggest a regulatory role of TNTs in the pathological bone destruction.

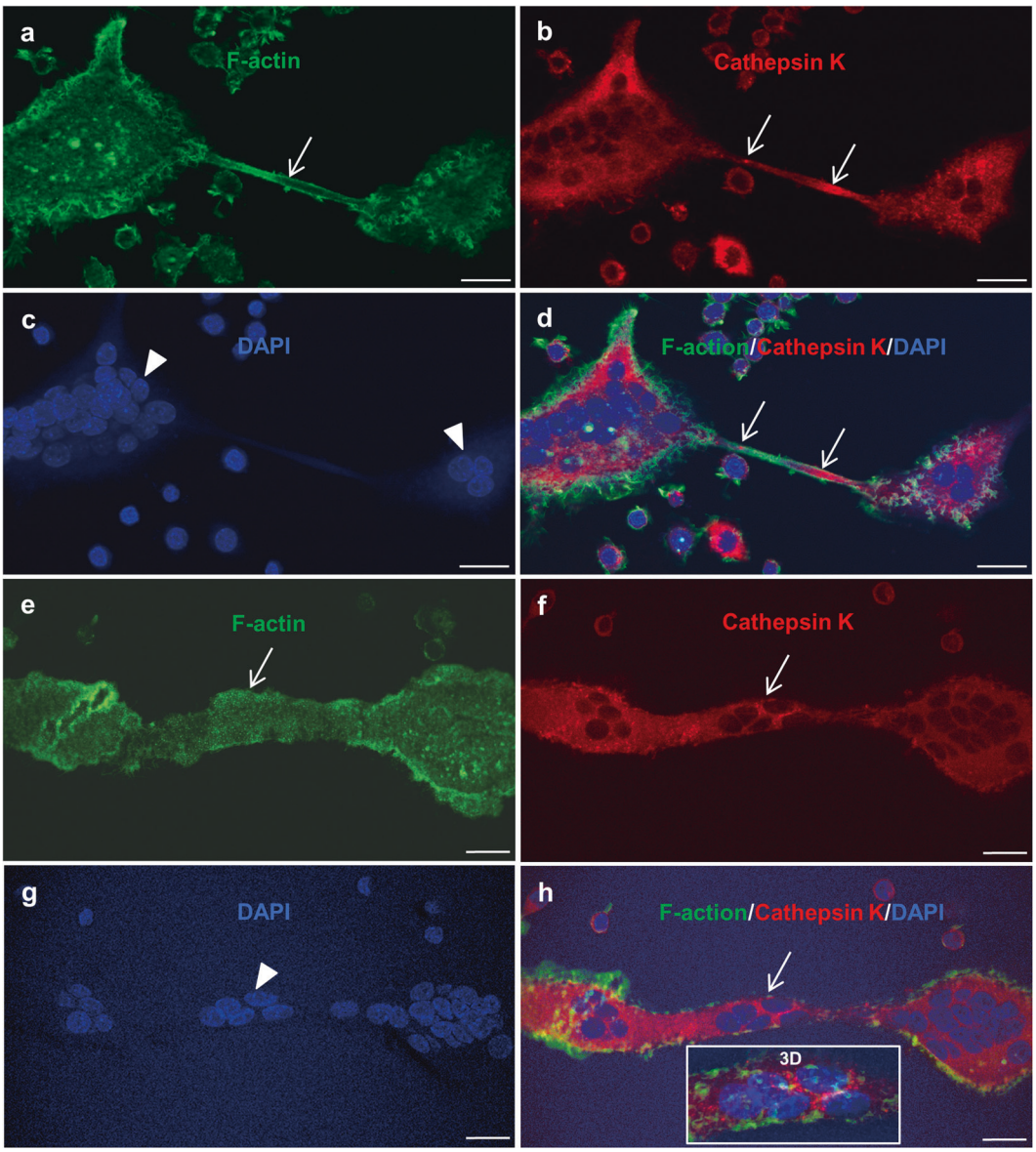

Fig. 6 Immunofluorescence detection of co-distribution of F-actin and Cathepsin K in TNT observed in osteoclastogenesis in RAW-D cell culture. a–h The medium and thick TNTs were observed between two multinucleated osteoclast-like cells (arrows). Co-distribution of F-actin (**a**, **e** green) and Cathepsin K (**b**, **f** red) was observed in the actin-based TNT and connected osteoclast-like cells. Some Cathepsin K-positive vesicular components were present in the medium size TNT formed between osteoclasts (**b**, **d** arrows). Nuclei were detected by DAPI (**c**, **g** blue, arrowheads). **e–h** A thick intercellular bridge formed between multinucleated osteoclast-like cells. Several nuclei were observed in the intercellular bridge (**f–h**). The three-dimensional view of the arrowed area was shown in the inset of (**h**). **d**, **h** Merged images of the F-actin, Cathepsin K, and nuclei in TNT formed between connected osteoclast-like cells. Scale bars: 20 μm (**a–h**).

TNT-like structures with 50–800 nm in diameter are recognized to be responsible for transferring molecules or organelles among connecting cells[18,34,35]. According to the previous report, thin TNTs (<0.7 μm) possess actin filaments, while thick TNTs (>0.7 μm) have both of actin filaments and microtubules[36]. The thick TNTs can transport organelles and macromolecules, thereby facilitating intercellular communication, synchronization of cell division and differentiation and coordination of cell behavior during development[37]. Thus, TNTs are recognized to play an important role in most of the physiological and pathological aspects of multicellular organisms[8,13,20,38]. In the present study, we classified the TNTs formed in osteoclastogenesis into three types: thin, medium, and thick TNT, depending on the diameter and length of TNTs. To date, researchers have mainly focused on the thin nanotubes, but the TNT could be represented by different types, such as cytonemes, intercellular micrometer-level tubes, or intercellular bridges[18,25]. We propose here that the types of TNTs are categorized into three types according to their diameter, length, and the type of connecting cells. TNTs involved in osteoclastogenesis could be dynamically changed from thin to thick dependent on the stage of cell differentiation. In the current observations, thin TNTs <300 nm were frequently observed in e-OCPs and they may target or communicate with specific cells or the same type of cells. TNTs bridging between mononuclear l-OCP or multinucleated osteoclasts are the medium and thick TNTs with the diameter of larger than 300 nm. Particularly, medium TNTs with a diameter around 300–800 nm were sometimes quite long and connected two remote cells without attaching several adjacent cells. Such TNTs are supposed to be formed probably to find the real fusion partner cells. Although few thick TNTs were observed, the diameter of

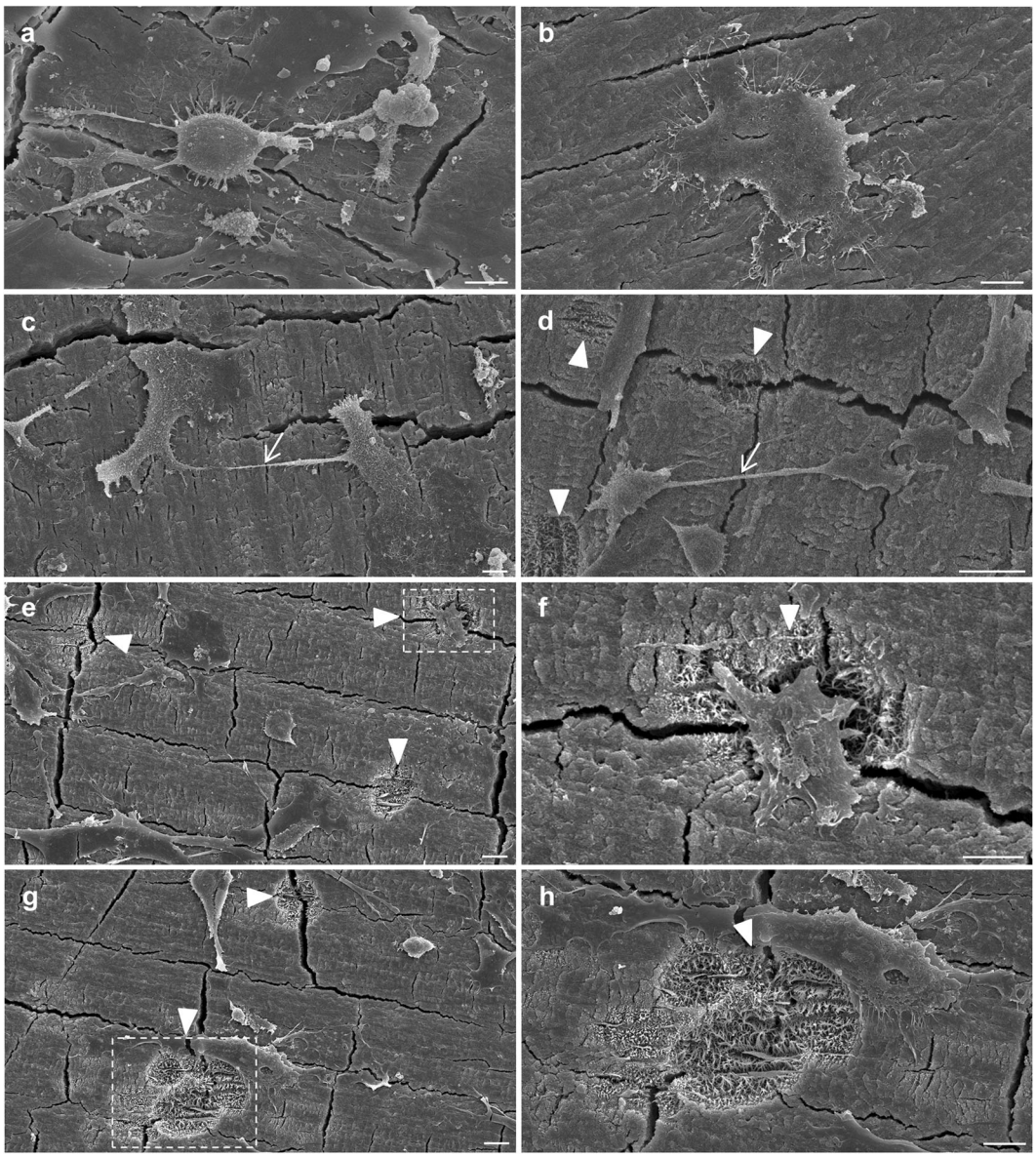

Fig. 7 TNT-mediated interaction among primary osteoclasts cultured on calcified matrices. BMMs were stimulated to form osteoclasts in the presence of M-CSF and RANKL and replated on dentin slices followed by culture for 2 or 3 days as described in Materials and Methods. **a** A small osteoclast with numerous protrusions toward the dentin surface. **b** Osteoclast with irregular shape observed on the dentin slice. **c**, **d** Relatively thick TNT observed between two osteoclasts (arrow). **d–h** Apparent resorption lacunae were also observed on the surface of the dentin slice (arrowheads). **f** The resorption lacunae associated with osteoclast. **g** Typical resorption lacunae with clusters of smaller and larger size of lacunae observed on the surface of the dentin slice, in which collagen fibrils were observed on the floor of resorption lacunae. **f**, **h** are the high magnification views of the boxed areas of (**e** and **g**), respectively. Scale bars: 10 μm (**a–h**).

TNTs is likely to be thicker, at around 800 nm–2.5 μm just prior to fusion, among osteoclast precursors. Such thicker TNTs would be quite useful for transport large cellular components including cell membrane organelles and nuclei in prior to cell fusion. These findings are consistent with our previous observation by time-lapse imaging analysis[22]. The different diameter in the type of TNTs could be reflecting substances involved in each TNT. In fact, our previous[22] and current studies showed transfer of the membrane molecules in the thin TNTs and the presence of beaded bulges in the medium TNTs which are related to the transport larger organelles. We further demonstrated the dramatic migration of nuclei through the thicker TNTs during osteoclast formation. These results strongly suggest that multinucleated osteoclasts are formed by fusion of osteoclast precursors through the active movement of organelles and nuclei via TNT-like structures.

Interestingly, we found the presence of several side branches in some medium and thick TNTs. Such side branches may physically fix the position and direction of long TNTs or drive the cell migration. We have also found that some side branches of TNT were likely to interact with fine cellular protrusions of the adjacent cells. In an extreme case, such side branches connected with multiple osteoclast precursors, which could contribute to the efficient formation of large multinuclear osteoclasts. As we have utilized a pure population of osteoclast precursors by use of the RAW-D cell line in most of the data for the cell surface morphological analysis during osteoclastogenesis, all observed events in RAW-D cell cultures are exactly those of cells in the osteoclast-lineage. So far, few SEM analysis have been reported concerning the surface morphological changes during osteoclast differentiation[24,39], our current observations demonstrate for the

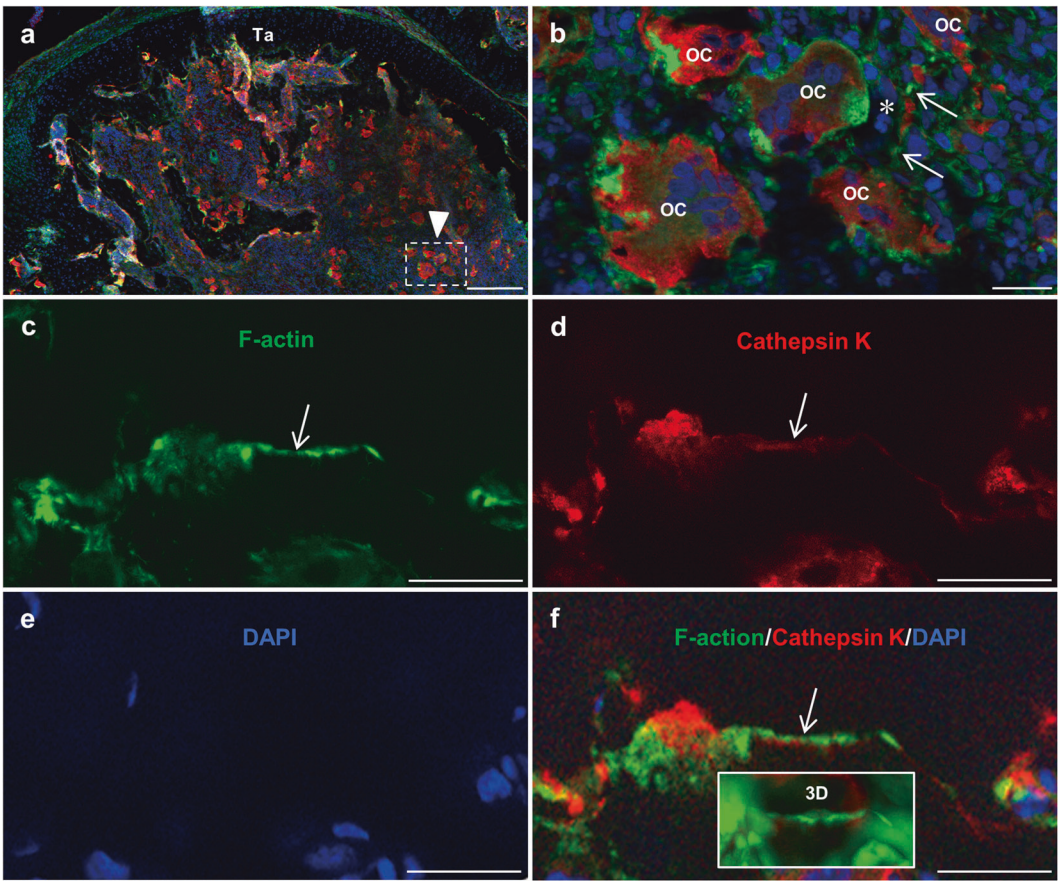

Fig. 8 In vivo detection of TNT-like intercellular bridges among pathological multinucleated osteoclasts in rats with adjuvant-induced arthritis. a Numerous large osteoclast observed in bone destruction sites in talus in rats with adjuvant-induced arthritis. F-actin and Cathepsin-K were immunohistochemically detected. **b** A high magnification view of the boxed area of (**a**) (arrowhead), in which cluster of abundant multinucleated osteoclasts were present. **c–f** Show the higher magnification views of TNT (arrows) observed in the asterisked area of (**b**). Localizations of F-actin (green) (**c**), Cathepsin K (red) (**d**) and nuclei (blue) (**e**) were shown respectively. **f** Shows the merged image of (**c**, **d** and **e**). Inset of (**f**) shows a three-dimensional view of the arrowed area of (**f**), in which the TNT formed between two osteoclasts was observed. Ta: Talus, OC: multinucleated osteoclast, Scale bars: 200 μm (**a**), 20 μm (**b–f**).

first time the detailed morphological changes of osteoclast-like cells and TNTs during osteoclastogenesis by use of SEM analysis. Our findings could provide a deep impact on the understanding of the detailed cellular events in osteoclast differentiation.

Two types of TNT have been reported that connect TNTs and the cell body[36]. One is the close-ended TNT, with junctions, and the other is the open-ended TNT, without junctions. We did not detect any special structures at the joint between TNTs and cells in osteoclast formation. In our previous reports, membrane lipids stained with immunofluorescent DiI were shown to move back and forth on the surface of TNTs formed between two osteoclast precursors[22]. Our current results of SEM analysis indicate that TNTs during osteoclastogenesis are those of the open-ended type. The reason for the presence of different connection types in TNT is not yet known, however, it could be partially due to the difference in the connecting cell types. Immunofluorescent staining and electron microscopic analysis have revealed the involvement of actin filaments, microtubules, and intermediate filaments in TNTs, especially in thick TNT[25,40,41]. Intercellular substance transport occurs when the beaded bulges are formed, and such transportation is realized by the cooperative actions of actin filaments with microtubules or with intermediate filaments present in TNTs. It has also been reported that actin-rich micrometer-level tubes in osteoclasts exchange organelles, even including nuclei[24,25].

Since TNTs are found in cells in the human immune system and in mesenchymal stem cells in vivo[11,42–44] and intercellular bridges are also observed by live imaging of bone[45] and muscle[46], TNT formation is a generally accepted phenomenon, which is not only observed under normal homeostatic conditions but also in pathological states in vivo[13,20]. We have analyzed the formation of TNTs in primary osteoclasts cultured on dentin slices and detected typical TNTs between two active multinuclear osteoclasts bearing bone resorbing activity. These findings strongly suggest that osteoclasts are communicating each other by use of TNTs. Mature osteoclasts could interact each other to modulate bone resorbing function or migration activity through the tunneling intercellular bridges. In the inflammatory bone destruction sites of rats with AA, we have successfully detected TNT-like structures formed between osteoclasts. Pathologically activated osteoclasts also could communicate each other through TNTs to modulate bone destruction. TNTs in osteoclast-like cells become thicker and shorter before cell fusion. When small osteoclast precursors were attracted toward the main large cell, thicker intercellular bridges were formed prior to fusion among osteoclast precursors. Furthermore, multinucleated osteoclasts can protrude short processes to their peripheral area and incorporate into the surrounding cells by cell-cell fusion to become giant multinucleated osteoclast-like cells. In the present study, we have demonstrated that TNT-mediated intercellular communication is important in cell fusion process in osteoclast differentiation. Formation and elongation of TNTs are regulated by tumor necrosis factor-α-induced protein 2 (TNFaip2, also known as M-Sec) gene products which regulate the polymerization of actin and movement of membrane vesicles to cellular processes[47]. We have found

that RANKL-induced DC-STAMP is essential for osteoclastogenesis[23]. Now DC-STAMP is widely recognized as a key transmembrane molecule in fusion of osteoclast precursors[23,48]. In our previous study, we have reported a dynamic movement of DC-STAMP through TNTs is required for osteoclastogenesis, especially in the cell fusion of osteoclast precursors. We have shown that GFP-tagged DC-STAMP was actively transported between osteoclast precursors through TNTs[22,23]. Inhibition of M-Sec, or DC-STAMP movement may suppress functional TNT formation and osteoclastogenesis. In addition, destruction of TNT formation by use of Latrunculin B, an inhibitor of actin polymerization, inhibited osteoclast differentiation in vitro[22,24]. These results, together with our current findings, reinforce the notion that it is possible to suppress pathological osteoclastogenesis and bone destruction by inhibiting or disrupting the formation of TNTs in the pathological bone destruction sites in vivo. Further studies are required concerning in vivo regulation of osteoclastic bone resorption through modulating the formation of TNTs associated with osteoclasts.

DATA AVAILABILITY

All data generated and analyzed in this study are available.

REFERENCES

1. Zaidi, M. Skeletal remodeling in health and disease. *Nat. Med.* **13**, 791–801 (2007).
2. Feng, X. & McDonald, J. M. Disorders of bone remodeling. *Annu. Rev. Pathol.* **6**, 121–145 (2011).
3. Amarasekara, D. S. et al. Regulation of osteoclast differentiation by cytokine networks. *Immun. Netw.* (2018). https://doi.org/10.4110/in.2018.18.e8
4. Yoshida, H. et al. The murine mutation osteopetrosis is in the coding region of the macrophage colony stimulating factor gene. *Nature* **345**, 442–444 (1990).
5. Scheven, B. A., Visser, J. W. & Nijweide, P. J. In vitro osteoclast generation from different bone marrow fractions, including a highly enriched hematopoietic stem cell population. *Nature* **321**, 79–81 (1986).
6. Vignery, A. Macrophage fusion: the making of osteoclasts and giant cells. *J. Exp. Med.* **202**, 337–340 (2005).
7. Miyamoto, T. Regulators of osteoclast differentiation and cell-cell fusion. *Keio J. Med.* **60**, 101–105 (2011).
8. Rustom, A., Saffrich, R., Markovic, I., Walther, P. & Gerdes, H. H. Nanotubular highways for intercellular organelle transport. *Science* **303**, 1007–1010 (2004).
9. Koyanagi, M., Brandes, R. P., Haendeler, J., Zeiher, A. M. & Dimmeler, S. Cell-to-cell connection of endothelial progenitor cells with cardiac myocytes by nanotubes: a novel mechanism for cell fate changes? *Circ. Res.* **96**, 1039–1041 (2005).
10. Kimura, S., Hase, K. & Ohno, H. Tunneling nanotubes: emerging view of their molecular components and formation mechanisms. *Exp. Cell Res.* **318**, 1699–1706 (2012).
11. Liu, K. et al. Mesenchymal stem cells rescue injured endothelial cells in an in vitro ischemia-reperfusion model via tunneling nanotube like structure-mediated mitochondrial transfer. *Microvasc. Res.* **92**, 10–18 (2014).
12. Baler, M. How the internet of cells has biologists buzzing. *Nature* **549**, 322–324 (2017).
13. Winkler, F. & Wick, W. Harmful networks in the brain and beyond. *Science* **359**, 1100–1101 (2018).
14. Gurke, S. et al. Tunneling nanotube (TNT)-like structures facilitate a constitutive, actomyosin-dependent exchange of endocytic organelles between normal rat kidney cells. *Exp. Cell Res.* **314**, 3669–3683 (2008).
15. Sun X. et al. Tunneling-nanotube direction determination in neurons and astrocytes. *Cell Death Dis.* (2012). https://doi.org/10.1038/cddis.2012.177
16. Yasuda, K. et al. Tunneling nanotubes mediate rescue of prematurely senescent endothelial cells by endothelial progenitors: exchange of lysosomal pool. *Aging (Albany NY)* **3**, 597–608 (2011).
17. Domhan, S. et al. Intercellular communication by exchange of cytoplasmic material via tunneling nano-tube like structures in primary human renal epithelial cells. *PLoS ONE* (2011). https://doi.org/10.1371/journal.pone.0021283
18. Korenkova, O., Pepe, A. & Zurzolo, C. Fine intercellular connections in development: TNTs, cytonemes, or intercellular bridges? *Cell Stress* **4**, 30–43 (2020).
19. Yamashita, Y. M., Inaba, M. & Buszczak, M. Specialized intercellular communications via cytonemes and nanotubes. *Annu. Rev. Cell Dev. Biol.* **34**, 59–84 (2018).
20. Mittal, R. et al. Cell communication by tunneling nanotubes: implication in disease and therapeutic applications. *J. Cell Physiol.* **234**, 1130–1146 (2019).
21. Pal, R. R. et al. Pathogenic *E. coli* extracts nutrients from infected host cells utilizing injectisome components. *Cell* **177**, 683–696 (2019).
22. Takahashi, A. et al. Tunneling nanotube formation is essential for the regulation of osteoclastogenesis. *J. Cell Biochem.* **114**, 1238–1247 (2013).
23. Kukita, T. et al. RANKL Induced DC-STAMP is essential for osteoclastogenesis. *J. Exp. Med.* **200**, 941–946 (2004).
24. Li, R. F., Zhang, W., Man, Q. W., Zhao, Y. F. & Zhao, Y. Tunneling nanotubes mediate intercellular communication between endothelial progenitor cells and osteoclast precursors. *J. Mol. Histol.* **50**, 483–491 (2019).
25. Pennanen, P. et al. Diversity of actin architecture in human osteoclasts: network of curved and branched actin supporting cell shape and intercellular micrometer-level tubes. *Mol. Cell Biochem.* **432**, 131–139 (2017).
26. Watanabe, T. et al. Direct stimulation of osteoclastogenesis by MIP-1α: evidence obtained from studies using RAW264 cell clone highly responsive to RANKL. *J. Endocrinol.* **180**, 193–201 (2004).
27. Kukita, T., Takahashi, A., Zhang, J. Q., Kukita, A. Membrane nanotube formation in osteoclastogenesis. (Pfannkuche K., eds). *Methods mol biol, cell fusion: overviews and methods* 2nd edn, p. **1313**, 193–202 (Springer Science Business Media, 2015).
28. Takahashi, N., Udagawa, N., Tanaka, S., Suda, T. Generating murine osteoclasts from bone marrow. (Helfrich M. H., Ralston S. H., eds). *Methods Mol Med, Bone Research Protocols*. p. **80**, 129–144 (Humana Press Inc, 2003).
29. Kukita, A. et al. The transcription factor FBI-1/OCZF/LRF is expressed in osteoclasts and regulates RANKL-induced osteoclast formation in vitro and in vivo. *Arthritis Rheum.* **63**, 2744–2754 (2011).
30. Shiratori, T. et al. IL-1β Induces pathologically activated osteoclasts bearing extremely high levels of resorbing activity: A possible pathological subpopulation of osteoclasts accompanied by suppressed expression of Kindlin-3 and Talin-1. *J. Immunol.* **200**, 218–228 (2018).
31. Li, Y. J. et al. A possible suppressive role of galectin-3 in upregulated osteoclastogenesis accompanying adjuvant induced arthritis in rats. *Lab. Investig.* **89**, 26–37 (2009).
32. Kuratani, T. et al. Induction of abundant osteoclast-like multinucleated giant cells in adjuvant arthritic rats with accompanying disordered high bone turnover. *Histol. Histopathol.* **13**, 751–759 (1998).
33. Kukita, A. et al. Infection of RANKL-primed RAW-D macrophages with *Porphyromonas gingivalis* promotes osteoclastogenesis in a TNF-α-independent manner. *PLoS ONE* (2012). https://doi.org/10.1371/journal.pone.0038500
34. Austefjord, M. W., Gerdes, H. H., Wang, X. Tunneling nanotubes: diversity in morphology and structure. *Commun. Integr. Biol.* (2014). https://doi.org/10.4161/cib.27934
35. Mattes, B. & Scholpp, S. Emerging role of contact-mediated cell communication in tissue development and diseases. *Histochem. Cell Biol.* **150**, 431–442 (2018).
36. Onfelt, B. et al. Structurally distinct membrane nanotubes between human macrophages support long-distance vesicular traffic or surfing of bacteria. *J. Immunol.* **177**, 8476–8483 (2006).
37. Haglund, K., Nezis, I. P. & Stenmark, H. Structure and functions of stable intercellular bridges formed by incomplete cytokinesis during development. *Commun. Integr. Biol.* **4**, 1–9 (2012).
38. Thayanithy, V., Dickson, E. L., Steer, C., Subramanian, S. & Lou, E. Tumor-stromal cross talk: direct cell-to-cell transfer of oncogenic microRNA via tunneling nanotubes. *Transl. Res.* **164**, 359–365 (2014).
39. Domon, T. et al. Ultrastructural study of cell-cell interaction between osteoclasts and osteoblasts/stroma cells in vitro. *Ann. Anat.* **184**, 221–227 (2002).
40. Resnik, N. et al. Helical organization of microtubules occurs in a minority of tunneling membrane nanotubes in normal and cancer urothelial cells. *Sci. Rep.* (2018). https://doi.org/10.1038/s41598-018-35370-y
41. Sartori-Rupp, A. et al. Correlative cry-electron microscopy reveals the structure of TNTs in neuronal cells. *Nat. Commun*. (2019). https://doi.org/10.1038/s41467-018-08178-7
42. Inaba, M., Buszczak, M. & Yamashita, Y. M. Nanotubes mediate niche-stem cell signaling in the Drosophila testis. *Nature* **523**, 329–332 (2015).
43. Gong, J., Chen, D., Kashiwaba, M. & Kufe, D. Induction of antitumor activity by immunization with fusions of dendritic and carcinoma cell. *Nat. Med.* **3**, 558–561 (1997).
44. Vassilopoulos, G., Wang, P. R. & Russell, D. W. Transplanted bone marrow regenerates liver by cell fusion. *Nature* **422**, 901–904 (2003).
45. Ishii, M., Fujimori, S., Kaneko, T. & Kikuta, J. Dynamic live imaging of bone: opening a new era with 'bone histodynametry'. *J. Bone Miner. Metab.* **31**, 507–511 (2013).
46. Rehberg, M. et al. Intercellular transport of nanomaterials is mediated by membrane nanotubes in vivo. *Small* **12**, 1882–1890 (2016).
47. Hase, K. et al. M-Sec Promotes membrane nanotube formation by interacting with Ral and the exocyst complex. *Nat. Cell Biol.* **11**, 1427–1432 (2009).
48. Yagi, M. et al. DC-STAMP is essential for cell-cell fusion in osteoclasts and foreign body giant cells. *J. Exp. Med.* **202**, 345–351 (2005).

ACKNOWLEDGEMENTS

The authors thank Dr. Mizuho Kido of Saga University, Faculty of Medicine for helpful suggestions.

AUTHOR CONTRIBUTIONS

J.Z. performed experiments and analyzed the data by use of SEM; This study was conceived and designed by J.Z. and T.K.; A.T., J.G., Y.K. and X.Z. performed primary bone marrow cells isolation and culture, in vitro experiments, collection and assembly of data; The paper writing and figure design were performed by J.Z. and T.K.; A.K., N.U., H.H. and T.Y. deeply discussed on all data; All authors reviewed and accepted the final version of the paper.

FUNDING

This study was supported in part by a Grant for Scientific Research from Ministry of Education, Culture, Sports, Science and Technology of Japan (MEXT)/Japan Society for the Promotion of Science (JSPS) (16K11447, 18K09506).

COMPETING INTERESTS

The authors declare no competing interests.

ETHICAL APPROVAL

All animal experiments were performed according to the protocol approved by the Laboratory Animal Care and Use Committee of Kyushu University (No. A19-270-0).

ADDITIONAL INFORMATION

Correspondence and requests for materials should be addressed to Toshio Kukita.